REPORT DOCUMENTATION PAGE

Form Approved
OMB No. 0704-0188

1. AGENCY USE ONLY (Leave blank)	2. REPORT DATE	3. REPORT TYPE AND DATES COVERED
	31, July 1997	Technical 6/1/96 - 7/31/96

4. TITLE AND SUBTITLE
Spectroscopic, Voltammetric, and Electrochemical Scanning Tunneling Microscopic Study of Underpotentially Deposited Cu Corrosion and Passivation with Self-Assembled Organomercaptan Monolayers

5. FUNDING NUMBERS
N00014-93-11338
300x084yip
96PR0-1027

6. AUTHOR(S)
F. P. Zamborini, J. K. Campbell, R. M. Crooks

7. PERFORMING ORGANIZATION NAME(S) AND ADDRESS(ES)
Department of Chemistry
Texas A&M University
College Station, Texas 77843-3255

8. PERFORMING ORGANIZATION REPORT NUMBER
27

9. SPONSORING/MONITORING AGENCY NAME(S) AND ADDRESS(ES)
Office of Naval Research
800 North Quincy Street
Arlington, Virginia 22217-5000

10. SPONSORING/MONITORING AGENCY REPORT NUMBER

11. SUPPLEMENTARY NOTES
Submitted for publication in *Langmuir*.

12a. DISTRIBUTION/AVAILABILITY STATEMENT
Reproduction in whole, or in part, is permitted for any purpose of the United States Government. This document has been approved for public release and sale; it's distribution is unlimited.

12b. DISTRIBUTION CODE

13. ABSTRACT *(Maximum 200 words)*

FTIR-external reflectance spectroscopy (FTIR-ERS), x-ray photoelectron spectroscopy (XPS), electrochemistry, and electrochemical scanning tunneling microscopy (ECSTM) were used to study the effect of thiol adsorbates on the oxidation of underpotentially deposited Cu on Au (Au/Cu-UPD) in $HC1O_4$-containing electrolyte solutions. The morphology of the corroding Cu layer and its stripping potential are influenced by the presence of the thiol monolayers. Hexadecanethiol prevented corrosion of Cu-UPD up to potentials more than 1200 mV positive of its oxidation potential on unpassivated electrodes. 4-hydroxythiophenol and pentanethiol also shift the oxidation potential but to a lesser degree. These findings raise the possibility for new strategies to prevent corrosion using very thin, easily prepared composite films.

14. SUBJECT TERMS

15. NUMBER OF PAGES
30

16. PRICE CODE

17. SECURITY CLASSIFICATION OF REPORT	18. SECURITY CLASSIFICATION OF THIS PAGE	19. SECURITY CLASSIFICATION OF ABSTRACT	20. LIMITATION OF ABSTRACT
Unclassified	Unclassfied	Unclassfied	

[Prepared for publication as an Article in *Langmuir*]

Spectroscopic, Voltammetric, and Electrochemical Scanning Tunneling Microscopic Study of Underpotentially Deposited Cu Corrosion and Passivation with Self-Assembled Organomercaptan Monolayers

Francis P. Zamborini, Joseph K. Campbell, and Richard M. Crooks*,[1]

Department of Chemistry

Texas A&M University

College Station, TX 77843-3255

[1]e-mail: crooks@chemvx.tamu.edu; fax: 409-845-1399; voice: 409-845-5629

*Author to whom correspondence should be addressed.

Submitted: August 6, 1997

Abstract

FTIR-external reflectance spectroscopy (FTIR-ERS), x-ray photoelectron spectroscopy (XPS), electrochemistry, and electrochemical scanning tunneling microscopy (ECSTM) were used to study the effect of thiol adsorbates on the oxidation of underpotentially deposited Cu on Au (Au/Cu-UPD) in $HClO_4$-containing electrolyte solutions. The morphology of the corroding Cu layer and its stripping potential are influenced by the presence of the thiol monolayers. Hexadecanethiol prevented corrosion of Cu-UPD up to potentials more than 1200 mV positive of its oxidation potential on unpassivated electrodes. 4-hydroxythiophenol and pentanethiol also shift the oxidation potential but to a lesser degree. These findings raise the possibility for new strategies to prevent corrosion using very thin, easily prepared composite films.

Introduction

We report a spectroscopic, voltammetric, and electrochemical scanning tunneling microscopic (ECSTM) study of the corrosion passivation properties of aromatic and linear-chain organomercaptan self-assembled monolayers (SAMs) on Cu electro-oxidation in aqueous $HClO_4$. This study follows our earlier examination of corrosion passivation of Au by SAMs in the presence of CN^- and Br^-.[1,2] We have chosen to work with underpotentially deposited Cu (Cu-UPD) on Au(111) substrates for two reasons. First, the Au(111)/Cu-UPD system is especially good for studying the very early stages of Cu corrosion since it is possible to visualize the time-dependent dissolution of exactly one atomic layer of Cu. This is particularly useful for ECSTM studies since without a stop-etch layer (Au in the present case) it is difficult to know the total number of layers etched. Second, recent studies by Jennings and Laibinis show that UPD layers of Ag and Cu stabilize SAM adlayers.[3,4] Therefore, this approach also permits us to learn how different types of SAMs affect the initial stages of corrosion.

Cu is a commercially important metal because of its high thermal and electronic conductivity, high strength, and decorative appearance. Cu and its alloys are widely used in the electronics industry, in heating and cooling systems, for domestic water pipes, and in architectural metal-work.[5] Cu is a fairly noble metal, but reacts quickly in air to form a stable oxide. Corrosion of Cu can lead to pitting, staining,

or tarnishing of the surface. Accordingly, there is a great deal of interest in understanding the initial stages of Cu corrosion and determining new methods to passivate Cu surfaces.

The Au/Cu-UPD system has been studied previously in aqueous $HClO_4$[6,7] and H_2SO_4[7-13] electrolyte solutions by electrochemistry,[8,12] ECSTM,[6,9-11,13] electrochemical atomic force microscopy (ECAFM),[7] and other analytical methods.[12] Most of the studies involving *in-situ* scanning probe techniques have been focused on determination of the potential-dependent, atomic-resolution Cu adlayer structure. However, Green and Hanson[10] have studied the Cu-UPD and stripping processes on Au(111) at the nanometer scale in H_2SO_4 electrolytes containing Cu^{2+}.

There is a vast literature dealing with corrosion of Cu and its alloys under various conditions as studied by classic electrochemical techniques.[14-19] The few that use scanning probe techniques (AFM, STM) include corrosion studies of Cu or its alloys in ClO_4^-,[20] Cl^-,[21-24] and SO_4^{2-}.[25-28] Some of these are particularly relevant to the present study. For example, Suggs and Bard[22] used *in-situ* STM to study the corrosion of Cu(111) in aqueous Cl^- solution. At corrosive potentials, they found that etching occurred preferentially at step edges along the {211} direction. The use of organomercaptan SAMs as barriers towards Cu corrosion has also previously been reported. Whitesides *et al.* were the first to report on the properties of *n*-alkylthiol SAMs on

Cu.[29,30] They studied the air oxidation of Cu modified with SAMs of different chain lengths and found that the rates of oxidation of the Cu and the thiolates can be decreased approximately 50% by increasing the length of the SAM by four methylene units.[31] Moffat *et al.* found that the potential for global surface roughening of a Cu_3Au alloy was increased by adsorbing an *n*-alkylthiol SAM to the alloy.[28] Feng *et al.* studied the protection ability of a 1-dodecanethiol SAM on Cu surfaces that were pretreated in different ways.[32] They discovered that the passivation properties were enhanced by a nitric-acid etch of the Cu prior to SAM adsorption. A series of papers by Aramaki *et al.* examined the corrosion resistance of Cu coated with an 11-mercapto-1-undecanol SAM linked to a second polymeric alkyltrichlorosilane layer.[33-36] They used electrochemical and spectroscopic techniques to determine the protection efficiencies of the different films and found that the polymerized SAMs are more effective at preventing corrosion than long linear-chain SAMs such as octadecanethiol.

Recently, Jennings and Laibinis discovered that SAMs prepared on UPD layers of Cu and Ag on Au are highly organized and, most significantly, are more stable than SAMs formed on the parent metals.[3,4] This was demonstrated by measuring the extent of SAM desorption in aggressive, heated solvents and by adsorbate exchange-and-replacement experiments. Burgess and Hawkridge also studied the self assembly of octadecanethiol on Ag-UPD layers on Au using

electrochemical quartz crystal microbalance (ECQCM)-based gravimetry.[37] They found that the rate of self assembly was irreproducible on naked Au compared to that measured on a Ag-UPD overlayer. Although there have been several spectroscopic and electrochemical studies, to our knowledge this is the first *in-situ* corrosion passivation study of Cu by organomercaptan SAMs using electrochemical scanning probe techniques.

The goal of this study was to quantify the enhanced stability that different SAMs afford the Cu-UPD layer on Au and to determine the morphology of naked and thiol-modified Cu during the initial stages of corrosion. The Au/Cu-UPD electrodes were modified with monolayers of the following: $CH_3(CH_2)_4SH$, C5SH; HOC_6H_4SH, 4-HTP; $CH_3(CH_2)_{15}SH$, C16SH. The presence of the SAMs and Cu-UPD layers was verified using FTIR-external reflectance spectroscopy (FTIR-ERS) and x-ray photoelectron spectroscopy (XPS), respectively. Electrochemical and ECSTM results indicate that the potential of the UPD oxidation process and the morphology of the Cu while undergoing electro-oxidation is strongly dependent upon the type of SAM used.

Experimental Section

Chemicals. $CH_3(CH_2)_4SH$ (Aldrich, 98%), $HClO_4$ (Seastar, ultrapure), $Cu(ClO_4)_2$ (Aldrich, 98%), and 100% ethanol (Quantum Chemical Corp.) were used as received. 4-hydroxythiophenol, HOC_6H_4SH (Aldrich, 90%) was vacuum sublimed

and $CH_3(CH_2)_{15}SH$ (Aldrich, 92%) was distilled at reduced pressure. All aqueous solutions were prepared with deionized water (Millipore, Milli-Q purification system, resistance ≈ 18 MΩ-cm).

Substrate Preparation. Au-coated substrates for FTIR-ERS, XPS, and voltammetry were prepared by electron-beam deposition of 100 Å of Ti followed by 2000 Å of Au onto Si(100) wafers (Lance Goddard Assoc., Foster City, CA). The Au-coated Si wafers were cleaned in a low-energy Ar plasma cleaner at medium power for 1 min (Harrick Scientific Corp., New York, Model PDC-32G) immediately prior to use. ECSTM substrates were freshly prepared single-crystal Au(111) facets on gold beads, the preparation of which has been described previously.[38-43] Briefly, melting an Au wire (0.5-mm diameter, 99.99% purity, Refining Systems Inc., Las Vegas, NV) in a H_2/O_2 flame forms a 1.5-2.0 mm-diameter ball at the end of the wire. The ball has elliptical Au(111) facets (long axis ~300 μm) on its surface that contain atomically flat terraces up to 1 μm wide.

SAMs were formed on Cu-UPD layers as follows: After cleaning the Au wafers or Au beads, the substrates were immersed into a solution containing 0.01 M $Cu(ClO_4)_2$ and 0.1 M $HClO_4$ under potential control at 500 mV. The substrates were then cycled between 100 and 1500 mV at 20 mV/s until the Cu-UPD and the Au oxidation waves became well-defined. The substrates were then emersed at 50 mV while rinsing with water. Finally, the Au/Cu-UPD substrates were rinsed with

ethanol and quickly placed in the appropriate ethanolic organomercaptan solution (1-2 mM) and soaked for more than 24 h, except as noted. Upon removal from the thiol solution, the substrates were rinsed with ethanol and dried under a stream of nitrogen prior to use.

Electrochemical Measurements. All electrochemical measurements were performed using a Pine Instruments model AFCBP1 bipotentiostat (Grove City, PA). The data were recorded on a Kipp and Zonen X-Y recorder. The cell, fabricated from Kel-F, was designed to expose a 0.25 cm^2 working area of the Au wafer to the electrolyte solution. The approximately 15 mL cell volume accommodates a Pt counter electrode and an Ag/AgCl, 3 M NaCl, reference electrode (BAS, West Lafayette, IN) against which all potentials are reported. The substrates were immersed in air-saturated 0.1 M $HClO_4$ electrolyte solutions at -200 mV. For linear sweep voltammetry (LSV), the voltage was ramped at 10 mV/s and the first anodic scan was recorded past the Cu-UPD oxidation wave for the different electrodes. For cyclic voltammetry (CV), the voltage was cycled between -200 mV and 1500 mV stopping at -200 mV between successive scans.

FTIR-ERS Measurements. FTIR-ERS measurements were made using a Bio-Rad Digilab FTS-40 spectrometer equipped with a Harrick Scientific Seagull reflection accessory and a liquid-N_2-cooled MCT detector. All spectra were obtained using p-polarized light at an 84° angle of incidence with

respect to the substrate normal. Spectra are the sum of 256 or fewer individual scans.

XPS Measurements. XPS measurements were made using a Perkin-Elmer PHI 5500 spectrometer having a Mg anode at 400 W and pressures less than $7x10^{-8}$ mmHg. The pass energy was 29.35 eV with a 0.125 eV step size. Survey scans were acquired between 1100 and 0 eV and high-resolution scans were acquired for the relevant individual elements. Photoelectrons were detected at a 45° take-off angle. Each sample was exposed to the x-ray source for less than 1 h. All XPS peak positions were normalized to the Au ($4f_{7/2}$) peak at 84.0 eV.[3]

ECSTM Measurements. A Nanoscope III ECSTM (Digital Instruments, Santa Barbara, CA) equipped with an integral bipotentiostat was used for data acquisition. The tips were mechanically cut 80/20 Pt/Ir (Digital Instruments, Santa Barbara, CA) and coated with apiezon wax to minimize Faradaic current, which was typically 10-20 pA (measured by cycling the tip between +0.1 V and -0.1 V vs. a Pt wire in 0.1 M KCl). The 25 mL Kel-F ECSTM cell is large enough to accommodate a true reference electrode (Ag/AgCl, 3 M NaCl, BAS, West Lafayette, IN) against which all potentials are reported. A Pt wire counter electrode completed the cell.

All ECSTM images were obtained in the constant-current mode. The tip was biased 50 mV positive of the substrate. Scan rates of 3-5 Hz, which correspond to about 1 min per image, were used. All substrates were immersed at -200 mV

unless otherwise noted. For the Cu-UPD stripping experiments, once sharp images and minimal drift were observed, consecutive images were obtained at 25 mV potential increments, except at potentials of intermediate Cu-UPD coverages, where increments of 10 mV were used. Larger images were regularly acquired during each experiment to check for evidence of the tip perturbing the surface. The z-scale was 2 nm in all images and the tunneling current was varied between 200 pA and 1.0 nA. The potentials at which the images were acquired are noted in the figures.

Results and Discussion

Voltammetric Characterization. Figure 1 shows linear sweep voltammograms (LSV) obtained in 0.1 M $HClO_4$ of naked Au, Au/Cu-UPD, and the SAM-coated Au/Cu-UPD electrodes. The inset is a cyclic voltammogram (CV) obtained in the solution used to clean the Au and deposit the UPD layer of Cu prior to adsorption of the SAMs (see Experimental Section). The CV shows the Cu-UPD and stripping waves[8] on Au as well as the Au oxidation and reduction peaks (1200 mV and 900 mV, respectively). After the Cu-UPD and SAM adsorption, the LSVs were obtained for Cu-UPD stripping in $HClO_4$ solutions containing no Cu^{2+}.

Figure 1

For the naked Au electrode (Figure 1A), no anodic waves are observed as the potential is scanned positive from -200 mV to 900 mV. The cathodic background current observed at negative potentials is due to the reduction of O_2. The response of an Au/Cu-UPD electrode is shown in Figure 1B, where the Cu-UPD stripping wave is centered at 235 mV. This represents a 90 mV shift negative of the Cu-UPD stripping wave shown in the inset, which is a thermodynamic consequence of the absence of Cu^{2+} in all the solutions from which LSV data were obtained. The stripping wave for Au/Cu-UPD/C5SH is shifted to 595 mV (Figure 1C), 360 mV positive of Au/Cu-UPD. The Au/Cu-UPD/4-HTP stripping wave is present at 615 mV (Figure 1D). There is also a second peak in this LSV around 710 mV, which might correspond to Cu oxidation from a more passivated region of the electrode. The C16SH monolayer (Figure 1E) completely prevents the electro-oxidation of Cu up to at least 1500 mV. The current observed at the most extreme positive potentials probably corresponds to oxygen evolution, but XPS data discussed later confirms that the Cu-UPD layer remains on the surface. Also note the absence of a voltammetric signature for Au oxidation (see inset).

Figure 2 demonstrates that the passivating ability of C16SH immobilized on Au/Cu-UPD is far superior to that observed for naked Au. Figure 2A shows the cyclic voltammetry of the first, fifth, and tenth scan of Au/C16SH in 0.1 M $HClO_4$. On the first scan there is a very small current due to Au oxidation, indicating that C16SH largely

passivates the surface. By the tenth scan, however, the current increases significantly as the SAM becomes disordered and desorbs from the surface. Figure 2B contrasts this behavior with that observed for Au/Cu-UPD/C16SH, which protects the Au from surface oxidation remarkably well for at least ten scans. The results clearly indicate that the barrier properties of the SAM, and thus the corrosion passivation properties, improve markedly in the presence of the Cu-UPD adhesion layer.

Figure 2

FTIR-ERS Characterization. The FTIR-ERS spectra in Figure 3 confirm that the SAMs used in this study form on Au/Cu-UPD[3,4] and that, except for the case of the C16SH SAM, they are subsequently disordered or desorbed following large potential scans to where Cu-UPD oxidizes. The top IR spectrum in Figure 3A is of an Au/Cu-UPD/C5SH electrode, which is very similar to previously reported spectra of C3SH, C5SH, and C7SH on Au.[44-46] The peaks at 2964, 2936, and 2877 cm^{-1} arise from CH_3 modes. The absence of distinct bands attributable to asymmetric and symmetric CH_2 stretching modes between 2919-2925 and 2850-2855 cm^{-1}, respectively, may indicate that the monolayer is disordered and of lower coverage than is observed for the long-chain *n*-alkylthiols (Figure 3B).[44] Alternatively, the orientation of the methylene C-H dipoles may render them IR silent.[47] After a

potential scan from -200 mV to 900 mV in 0.1 M $HClO_4$ (bottom spectrum, Figure 3A), the symmetric CH_3 modes mostly disappear while the asymmetric CH_3 mode actually increases. In addition, the methylene asymmetric and symmetric peaks start to appear. This is consistent with the monolayer being highly disordered, of lower coverage, and in a conformation where the alkane-chain is near parallel to the surface plane.[47] This is anticipated since the underlying Cu-UPD has been oxidatively removed.

Figure 3

The top spectrum in Figure 3B shows the IR spectrum of Au/Cu-UPD/C16SH. The CH_3 modes are observed in the same locations as on the C5SH monolayer before Cu oxidation, but they are accompanied by asymmetric and symmetric CH_2 stretches at 2919 cm^{-1} and 2850 cm^{-1}, respectively, consistent with literature reports for highly ordered C16SH SAMs on Au.[44] This result is in contradistinction to previous reports for $CH_3(CH_2)_{17}SH$ on Au/Cu-UPD, where the asymmetric and symmetric CH_2 stretches were found to be shifted positive by 2-3 cm^{-1} towards less crystalline values.[3] This discrepancy can be attributed to different soaking times (40 min compared to 24 h in the present study) and possibly to the use of a different supporting electrolyte for Cu deposition: compared to H_2SO_4, $HClO_4$ has been found to lead to more close-packed Cu.[7] Consistent with Jennings and Laibinis,[3] we find that the

intensity of the asymmetric CH_2 stretch decreases for the C16SH monolayer on Au/Cu-UPD compared to C16SH on Au. They speculated that the decrease in intensity is due to less tilting of the alkane chain.[47] The bottom spectrum is the same surface after scanning from -200 mV to 1500 mV in 0.1 M $HClO_4$. In contrast to the Au/Cu-UPD/C5SH surface, there is little or no difference between the hydrocarbon regions in the top and bottom spectra. The CH_2 and CH_3 modes are located in the same position and are of nearly equal intensity. Together, with the previously discussed electrochemical data and the XPS data that follow, these data indicate that the SAM monolayer remains intact and highly ordered even after the large potential scan.

Figure 3C shows the IR spectrum of Au/Cu-UPD/4-HTP. The spectrum is similar to 4-HTP on Au,[48] except that all of the peaks are shifted to higher energy. For example, we observe the two aryl quadrant stretch modes at 1601 cm^{-1} and 1585 cm^{-1} in the Au/Cu-UPD/4-HTP spectrum, which occur at 1594 cm^{-1} and 1579 cm^{-1}, respectively, for Au/4-HTP. The C-OH stretch for Au/Cu-UPD/4-HTP is located at 1283 cm^{-1}, but shifted down in energy by 19 cm^{-1} to 1264 cm^{-1} for Au/4-HTP. We believe that these shifts are due to the Cu being more electropositive than Au,[49] resulting in the thiol carrying more electron density when adsorbed on Au/Cu-UPD than when adsorbed on naked Au. This additional electron density is distributed over the entire molecule with the majority residing in the Aryl-OH bond, hence the 19 cm^{-1} shift in the C-OH stretch. No

peaks were observed in the IR spectrum after scanning the Au/Cu-UPD/4-HTP surface from -200 mV to 1000 mV in 0.1 M $HClO_4$, therefore the spectrum was not included in the figure. The important point is that the IR data establishes the presence of the SAMs on Au/Cu-UPD, and that they are consistent with previous results. The results obtained for the surfaces after scanning to positive potentials, where Cu-UPD oxidizes, are consistent with the electrochemical data and the XPS data to follow.

XPS Characterization. The XPS data in Figure 4 confirm that the Cu-UPD layer survives the self-assembly process and that, except in the case of Au/Cu-UPD/C16SH, it is subsequently removed by electrochemical stripping. The spectrum of naked Au/Cu-UPD and the top spectra shown for the three pairs of SAM-modified electrodes show the Cu ($2p_{3/2}$) and ($2p_{1/2}$) peaks located at 931.1 and 950.8 eV, respectively, which indicate that the Cu is present either as Cu(0) or Cu(I). Unfortunately, XPS can't distinguish between these two possibilities.[50] The four-peak pattern characteristic of Cu(II) is definitely not observed.[51] The Cu XPS intensity decreases as the monolayer thickness increases, which is consistent with the findings of Bain and Whitesides for SAMs on Au.[52]. The lower spectra were obtained after immersing identically prepared electrodes into aqueous $HClO_4$ at -200 mV and scanning to 900 mV, 1000 mV, and 1500 mV for the C5SH-, 4-HTP-, and C16SH-modified Au/Cu-UPD surfaces, respectively. The spectra shown for the C5SH and 4-HTP surfaces show that

all of the Cu desorbs during the scan, while there is little or no loss of Cu from the Au/Cu-UPD/C16SH surface. This is consistent with the spectroscopic and electrochemical data, which support Cu-UPD stripping on the C5SH and 4-HTP surfaces, but not on the C16SH surface.

Figure 4

ECSTM Results. Figure 5 shows 300 nm x 300 nm ECSTM images of Au, Au/Cu-UPD, and SAM-modified Au/Cu-UPD electrodes obtained in aqueous 0.1 M $HClO_4$. At least one Au(111) atomic step edge (0.235 nm in height)[10,53] is included in each image as an internal reference for the z-scale normal to the surface. Figure 5A shows an unmodified Au(111) electrode at 200 mV. The surface reveals Au monoatomic steps and its features are stable up to around 600 mV, where Cl^- impurities (present in the $HClO_4$ electrolyte) adsorb strongly and enhance mobility of surface Au atoms, resulting in annealing.[54] At 800 mV (Figure 5B), Cl^- begins to dissolve the Au preferentially at step edges and other high energy defect sites, while the terraces remain unchanged. At 1000 mV (Figure 5C), which is near the foot of the Au oxidation wave, the potential is sufficiently positive to cause pitting by Cl^- on the terraces in addition to corrosion along the step edges. An oxide layer also forms slowly on the Au, which leads to passivation of the surface at more positive potentials. This data is significant because it shows that

in $HClO_4$, the Au surface does not change until potentials above 600 mV. In the following ECSTM images, we monitored the stripping of Cu-UPD layers in the potential range of -200 mV to 350 mV for the Au/Cu-UPD, Au/Cu-UPD/C5SH, and the Au/Cu-UPD/4-HTP surfaces. The control experiment represented by parts A-C of Figure 5 indicate that any morphology changes arise from the Cu-UPD layer, not the underlying Au.

Figure 5

Parts D-F of Figure 5 show the ECSTM images of an Au/Cu-UPD electrode over a potential range where Cu is electro-oxidized. Figure 5D shows the surface at -50 mV, corresponding to an almost full Cu-UPD coverage. Cu is represented by the lighter-colored domain-like islands uniformly distributed on the surface, while the darker regions correspond to the underlying Au surface. Figure 5E shows the same electrode at 150 mV where approximately half of the Cu-UPD layer remains. The Cu-UPD layer oxidizes homogeneously with no apparent topological preference for step edges or other specific sites, which is distinctly different from dissolution of bulk Cu(111) in Cl^-.[22] Figure 5F shows the same electrode at 200 mV after most of the Cu monolayer has dissolved. The raised circular island features gradually form as the last of the Cu-UPD layer corrodes. The islands are noticeably taller than the Cu-UPD domains in Figure 5E. The appearance of such islands has been

previously observed and attributed to a stable Cu (1 x 1) phase, which was measured to be higher above the Au surface than the other two phases observed for Cu-UPD on Au(111), and it required a larger overpotential to oxidize.[10] It is worth noting that the half-coverage potential according to our ECSTM data is approximately 85 mV negative of the Cu-UPD oxidation peak observed in the voltammetry (Figure 1B). We attribute this discrepancy to the many differences in the ECSTM and LSV experiments, such as scan rates, cell geometries, and substrates. This discrepancy exists in all of the ECSTM data. The important point is that the relative trends in the ECSTM data are in excellent agreement with the voltammetric results.

Parts G-I of Figure 5 show ECSTM images of an Au/Cu-UPD/C5SH electrode. Figure 5G was acquired at -75 mV with nearly a full Cu-UPD layer present. The image in Figure 5H is of the intermediate Cu coverage that exists at 210 mV. The corrosion process proceeds uniformly yielding a web-like structure of Cu, represented by the bright areas, covering the entire surface. The web-like strands are of near equal width and thickness and line-scans across them reveal that the Cu-Au step height is 0.10-0.12 nm, which is less than the Au-Au step height of approximately 0.24 nm. The Cu-Au step height is consistent with a Cu (5 x 5) adlattice structure,[10] provided that the C5SH monolayer does not significantly affect the electronic properties of the surface. High resolution images show that at intermediate coverages, no Cu

remains along step edges, suggesting that the Cu atoms along the step edges are in a chemically different environment than Cu atoms on the terraces. Note that on the naked surface (Figure 5F), nearly all of the Cu is dissolved at 200 mV, but the remainder of the Cu on the C5SH-coated surface does not fully strip until 290 mV (Figure 5I), leaving a surface decorated with a low density of monoatomic pits.

Parts J-L of Figure 5 show ECSTM data of an Au/Cu-UPD/4-HTP composite electrode. At -150 mV (Figure 5J), a complete Cu monolayer is stable on the Au surface. Figure 5K shows the same electrode having an intermediate Cu coverage at 300 mV. The corrosion of the Au/Cu-UPD/4-HTP occurs homogeneously throughout the surface with no apparent preference for one region over another. Although the surface also appears to be somewhat web-like, it is distinctly different from the C5SH-modified surface at a nearly equal Cu coverage (Figure 5H). The Cu remains in domains of various sizes, rather than web-like strands of equal width and height. Although the Cu coverage is similar to the C5SH-modified surface, the potential is 90 mV more positive, revealing that 4-HTP passivates the Cu more effectively (even though the monolayers are of approximately equal thickness). This trend is consistent with the voltammetry. Figure 5L shows the surface at 350 mV after most of the Cu is electro-oxidized. The potential is 60 mV more positive than on the C5SH surface (Figure 5I) yet some Cu still remains on the 4-HTP-modified surface. The potential is 150 mV more positive

than the naked Cu-UPD surface (Figure 5F), which had almost no Cu remaining at 200 mV.

Parts M-O of Figure 5 show the changes observed as the potential of an Au/Cu-UPD/C16SH composite electrode is stepped slowly positive. Figure 5M was obtained at -200 mV where there is full Cu coverage. It is interesting to note that the surface does not contain any of the monoatomic "thiol-induced pits" routinely observed in STM studies of long, linear-chain *n*-alkylthiol monolayers on Au(111), which is consistent with the enhanced stability of SAMs on the UPD surfaces.[40,55-57] Figure 5N was obtained at 475 mV, where there is still no indication of Cu-UPD stripping. The Cu layer remains unchanged on this surface at 775 mV (Figure 5O). Even at potentials as high as 1500 mV no further changes to the surface or evidence of Cu oxidation is apparent (data not shown). In addition to preventing the oxidation of Cu (1200 mV past its oxidation potential on naked Au(111)/Cu-UPD), this film even prevents dissolution of the Au by Cl^- and oxidation of the surface at potentials above 1100 mV. This finding was surprising, although consistent with the voltammetry, which showed no anodic current over this range.

The images of the Au/Cu-UPD/4-HTP and the Au/Cu-UPD/C16SH surfaces were acquired from different regions of the surfaces because the ECSTM tip appeared to disrupt these SAMs. Therefore, each image shown was acquired from a region of the surface that had not been previously imaged. Figure

6A shows an example of a tip effect that occurred on the C16SH-modified surface. The image was obtained at 900 mV after first imaging the center square region of 300 nm x 300 nm for several scans and then zooming out to 1 μm x 1 μm. During imaging of the square region, the surface appeared to be undergoing electrochemical changes. Upon zooming out, however, we observed that the surface was altered only under the area scanned by the tip. We believe that the square feature is due to disruption of the monolayer by the tip which selectively exposed the Cu and Au in that area to the corrosive conditions. We have previously observed this same effect on Au without a Cu-UPD layer.[2,58]

Figure 6

As was the case with the C16SH-modified electrode, the 4-HTP surface also showed evidence of the tip affecting the corrosion process (Figure 6B). The square feature with the vertically oriented large troughs was a previously imaged area. We believe that selective dissolution of the Cu occurs after scanning damages the protective SAM layer.

Conclusions

Previously, we demonstrated that organomercaptan SAMs retard the corrosion of metal surfaces. However, we concluded that SAMs were insufficiently stable to be of much technological significance. Following on the discovery of

Jennings and Laibinis that UPD layers of coinage metals greatly enhance SAM stability, we are more optimistic now about the commercial significance of these composite materials as ultrathin corrosion passivation layers. All of the monolayers, when formed on top of a Cu-UPD layer, shift the electro-oxidation of the Cu to more positive potentials relative to the untreated Cu-UPD layer. The morphology of the Cu during corrosion and the extent to which the Cu-UPD is passivated strongly depends upon the type of thiol adsorbed. The SAMs used here enhance metal passivation in the order: C16SH > 4-HTP > C5SH.

The amount of corrosion protection afforded to the UPD layer of Cu with extremely thin monolayers such as 4-HTP and C5SH (< 1.0 nm thick) is remarkable. Since the 4-HTP protects better than the C5SH, we conclude that (for short SAMs) aromatic or OH-terminated SAMs are superior to linear-chain or CH_3-terminated SAMs. The amount of protection gained by the longer C16SH (< 3.0 nm thick) on Cu-UPD is even more astonishing. Not only does the C16SH effectively passivate the Cu-UPD, but it also greatly enhances the nobility of the underlying Au. This strategy has real possibilities for increasing the corrosion resistance of protective coatings on more practical and commercially important metals.

Acknowledgment

We gratefully acknowledge the Office of Naval Research for full support of this work.

References and Notes

(1) Zamborini, F. P.; Crooks, R. M. *Langmuir*, submitted for publication.

(2) Zamborini, F. P.; Crooks, R. M. *Langmuir* **1997**, *13*, 122-126.

(3) Jennings, G. K.; Laibinis, P. E. *J. Am. Chem. Soc.* **1997**, *119*, 3208-3214.

(4) Jennings, G. K.; Laibinis, P. E. *Langmuir* **1996**, *12*, 6173-6175.

(5) Walker, R. *Anti-corrosion* **1970**, *17*, 9-15.

(6) Hotlos, J.; Magnussen, O. M.; Behm, R. J. *Surf. Sci.* **1995**, *335*, 129-144.

(7) Manne, S.; Hansma, P. K.; Massie, J.; Elings, V. B.; Gewirth, A. A. *Science* **1991**, *251*, 183-186.

(8) Omar, I. H.; Pauling, H. J.; Jüttner, K. *J. Electrochem. Soc.* **1993**, *140*, 2187-2192.

(9) Hachiya, T.; Honbo, H.; Itaya, K. *J. Electroanal. Chem.* **1991**, *315*, 275-291.

(10) Green, M. P.; Hanson, K. J. *J. Vac. Sci. Technol. A* **1992**, *10*, 3012-3018.

(11) Magnussen, O. M.; Hotlos, J.; Nichols, R. J.; Kolb, D. M.; Behm, R. J. *Phys. Rev. Lett.* **1990**, *64*, 2929-2932.

(12) Zhang, J.; Sung, Y.-E.; Rikvold, P. A.; Wieckowski, A. *J. Chem. Phys.* **1996**, *104*, 5699-5712.

(13) Möller, F. A.; Magnussen, O. M.; Behm, R. J. *Phys. Rev. B* **1995**, *51*, 2484-2490.

(14) Barcia, O. E.; Mattos, O. R.; Pebere, N.; Tribollet, B. *J. Electrochem. Soc.* **1993**, *140*, 2825-2832.

(15) Hack, H. P.; Pickering, H. W. *J. Electrochem. Soc.* **1991**, *138*, 690-695.

(16) Georgiadou, M.; Alkire, R. *J. Electrochem. Soc.* **1993**, *140*, 1340-1347.

(17) Brossard, L. *J. Electrochem. Soc.* **1983**, *130*, 403-405.

(18) Braun, M.; Nobe, K. *J. Electrochem. Soc.* **1979**, *126*, 1666-1671.

(19) Cooper, R. S.; Bartlett, J. H. *J. Electrochem. Soc.* **1958**, *105*, 109-116.

(20) Zhang, X. G.; Stimming, U. *Corros. Sci.* **1990**, *30*, 951-954.

(21) Morales, J.; Esparza, P.; Gonzalez, S. *Langmuir* **1996**, *12*, 500-507.

(22) Suggs, D. W.; Bard, A. J. *J. Am. Chem. Soc.* **1994**, *116*, 10725-10733.

(23) Suggs, D. W.; Bard, A. J. *J. Phys. Chem.* **1995**, *99*, 8349-8355.

(24) Kowal, K.; DeLuccia, J.; Josefowicz, J. Y.; Laird, C.; Farrington, G. C. *J. Electrochem. Soc.* **1996**, *143*, 2471-2481.

(25) Chan, H. S. O.; Ho, P. K. H.; Zhou, L.; Luo, N.; Ng, S. C.; Li, S. F. Y. *Langmuir* **1996**, *12*, 2580-2586.

(26) Pickering, H. W.; Wu, Y. C.; Gregory, D. S.; Geh, S. *J. Vac. Sci. Technol. B* **1991**, *9*, 976-983.

(27) Cruickshank, B. J.; Gewirth, A. A.; Rynders, R. M.; Alkire, R. C. *J. Electrochem. Soc.* **1992**, *139*, 2829-2832.

(28) Moffat, T. P.; Fan, F.-R. F.; Bard, A. J. *J. Electrochem. Soc.* **1991**, *138*, 3224-3235.

(29) Laibinis, P. E.; Whitesides, G. M.; Allara, D. L.; Tao, Y.-T.; Parikh, A. N.; Nuzzo, R. G. *J. Am. Chem. Soc.* **1991**, *113*, 7152-7167.

(30) Laibinis, P. E.; Whitesides, G. M. *J. Am. Chem. Soc.* **1992**, *114*, 1990-1995.

(31) Laibinis, P. E.; Whitesides, G. M. *J. Am. Chem. Soc.* **1992**, *114*, 9022-9028.

(32) Feng, Y.; Teo, W.-K.; Siow, K.-S.; Gao, Z.; Tan, K.-L.; Hsieh, A.-K. *J. Electrochem. Soc.* **1997**, *144*, 55-64.

(33) Itoh, M.; Nishihara, H.; Aramaki, K. *J. Electrochem. Soc.* **1994**, *141*, 2018-2023.

(34) Itoh, M.; Nishihara, H.; Aramaki, K. *J. Electrochem. Soc.* **1995**, *142*, 3696-3704.

(35) Itoh, M.; Nishihara, H.; Aramaki, K. *J. Electrochem. Soc.* **1995**, *142*, 1839-1846.

(36) Haneda, R.; Nishihara, H.; Aramaki, K. *J. Electrochem. Soc.* **1997**, *144*, 1215-1221.

(37) Burgess, J. D.; Hawkridge, F. M. *Langmuir* **1997**, *13*, 3781-3786.

(38) Schoer, J. K.; Ross, C. B.; Crooks, R. M.; Corbitt, T. S.; Hampden-Smith, M. J. *Langmuir* **1994**, *10*, 615-618.

(39) Snyder, S. R. *J. Electrochem. Soc.* **1992**, *139*, 5C.

(40) Ross, C. B.; Sun, L.; Crooks, R. M. *Langmuir* **1993**, *9*, 632-636.

(41) Chailapakul, O.; Crooks, R. M. *Langmuir* **1993**, *9*, 884-888.

(42) Hsu, T.; Cowley, J. M. *Ultramicroscopy* **1983**, *11*, 239-250.

(43) Sun, L.; Crooks, R. M. *J. Electrochem. Soc.* **1991**, *138*, L23-L25.

(44) Porter, M. D.; Bright, T. B.; Allara, D. L.; Chidsey, C. E. D. *J. Am. Chem. Soc.* **1987**, *109*, 3559-3568.

(45) Sun, L.; Kepley, L. J.; Crooks, R. M. *Langmuir* **1992**, *8*, 2101-2103.

(46) Chailapakul, O.; Sun, L.; Xu, C.; Crooks, R. M. *J. Am. Chem. Soc.* **1993**, *115*, 12459-12467.

(47) Porter, M. D. *Anal. Chem.* **1988**, *60*, 1143A-1155A.

(48) Xu, C.; Sun, L.; Kepley, L. J.; Crooks, R. M.; Ricco, A. J. *Anal. Chem.* **1993**, *65*, 2102-2107.

(49) *CRC Handbook of Chemistry and Physics*; 71st ed.; Lide, D. R., Ed.; CRC Press: Boston, 1990.

(50) *Practical Surface Analysis*; 2nd ed.; Briggs, D.; Seah, M. P., Eds.; John Wiley & Sons: New York, 1990; Vol. 1, pp 487-529.

(51) Wagner, C. D.; Kiggs, W. M.; Davis, L. E.; Moulder, J. F. *Handbook of X-ray Photoelectron Spectroscopy*; Perkin Elmer Corporation--Physical Electronics Division: Eden Prairie, MN, 1979.

(52) Bain, C. D.; Whitesides, G. M. *J. Phys. Chem.* **1989**, *93*, 1670-1673.

(53) Honbo, H.; Sugawara, S.; Itaya, K. *Anal. Chem.* **1990**, *62*, 2424-2429.

(54) Trevor, D. J.; Chidsey, C. E. D.; Loiacono, D. N. *Phys. Rev. Lett.* **1989**, *62*, 929-932.

(55) Sun, L.; Crooks, R. M. *Langmuir* **1993**, *9*, 1951.

(56) Kim, Y.-T.; Bard, A. J. *Langmuir* **1992**, *8*, 1096.

(57) Edinger, K.; Golzhauser, A.; Demota, K.; Woll, C.; Grunze, M. *Langmuir* **1993**, *9*, 4-8.

(58) Li, Y.-Q.; Chailapakul, O.; Crooks, R. M. *J. Vac. Sci. Technol. B* **1995**, *13*, 1-7.

Figure Captions

Figure 1: Linear sweep voltammograms of (A) Au (B) Au/Cu-UPD (C) Au/Cu-UPD/C5SH (D) Au/Cu-UPD/4-HTP and (E) Au/Cu-UPD/C16SH introduced into 0.1 M $HClO_4$ at -200 mV and scanned positive at 10 mV/s. The anodic peaks observed in (B), (C), and (D) results from oxidation of the Cu-UPD monolayer. The inset shows a typical voltammogram of Au and Cu-UPD oxidation and reduction. Voltammograms such as this were obtained prior to emersion at 50 mV and SAM formation.

Figure 2: Cyclic voltammograms obtained in 0.1 M $HClO_4$ of the first, fifth, and tenth scans between -200 mV and 1500 mV at 10 mV/s of (A) Au/C16SH and (B) Au/Cu-UPD/C16SH. The electrodes were soaked in the organomercaptan for 2-3 h prior to data acquisition. This comparison shows that the Cu-UPD layer adds to the stability of the SAM and leads to greater resistance towards Au oxidation.

Figure 3: FTIR-ERS spectra of (A) Au/Cu-UPD/C5SH (B) Au/Cu-UPD/C16SH (C) Au/Cu-UPD/4-HTP. Bottom spectra in (A) and (B) are after scanning from -200 mV to potentials of 900 mV and 1500 mV, respectively, in 0.1 M $HClO_4$ electrolyte. The C5SH spectrum shows significant loss of the CH_3 symmetric modes and a slight appearance of CH_2 modes, while the C16SH spectrum remains unchanged after the scan to positive potentials. The

spectrum of Au/Cu-UPD/4-HTP after scanning positive is not shown because no peaks were observed.

Figure 4: XPS spectra of Au/Cu-UPD and Au/Cu-UPD/SAM electrodes in the Cu (2p) region (top) before scanning to Cu-UPD oxidation potentials and (bottom) after scanning to Cu-UPD oxidation potentials. Each pair of spectra were obtained on two different substrates that were treated identically, except that the substrates used to obtain the bottom spectra of each pair were immersed into $HClO_4$ at -200 mV and scanned to 900 mV, 1000 mV, and 1500 mV on the Au/Cu-UPD/C5SH, Au/Cu-UPD/4-HTP, and Au/Cu-UPD/C16SH surfaces, respectively. It is apparent from the spectra before stripping that the Cu-UPD survives the self-assembly process. After stripping, Cu is absent in the C5SH and 4-HTP spectra, but the C16SH surface shows little or no Cu loss.

Figure 5: 300 nm x 300 nm ECSTM images obtained in 0.1 M $HClO_4$ of (A-C) Au; (D-F) Au/Cu-UPD; (G-I) Au/Cu-UPD/C5SH; (J-L) Au/Cu-UPD/4-HTP; (M-O) Au/Cu-UPD/C16SH. All potentials are referenced to Ag/AgCl, 3 M NaCl. The Au surface in (A-C) was introduced into the electrolyte at +200 mV, while the naked and SAM-modified Cu-UPD surfaces were introduced at -200 mV. Bias voltage was 50 mV and tunneling current ranged between 200 pA and 1.0 nA. Images in each row were not necessarily obtained in the same area of the surface because of tip effects described in the text.

Figure 6: ECSTM images showing tip effects that occurred during the Cu-UPD oxidation on surfaces composed of (A) Au/Cu-UPD/C16SH and (B) Au/Cu-UPD/4-HTP. The tip disrupts the surface in the scanned area making it impossible to obtain reliable data from the same area on subsequent scans throughout the experiment. The middle of each image is the area that was scanned prior to zooming out. The potentials were 900 mV and 200 mV for the C16SH- and 4-HTP-modified surfaces, respectively.

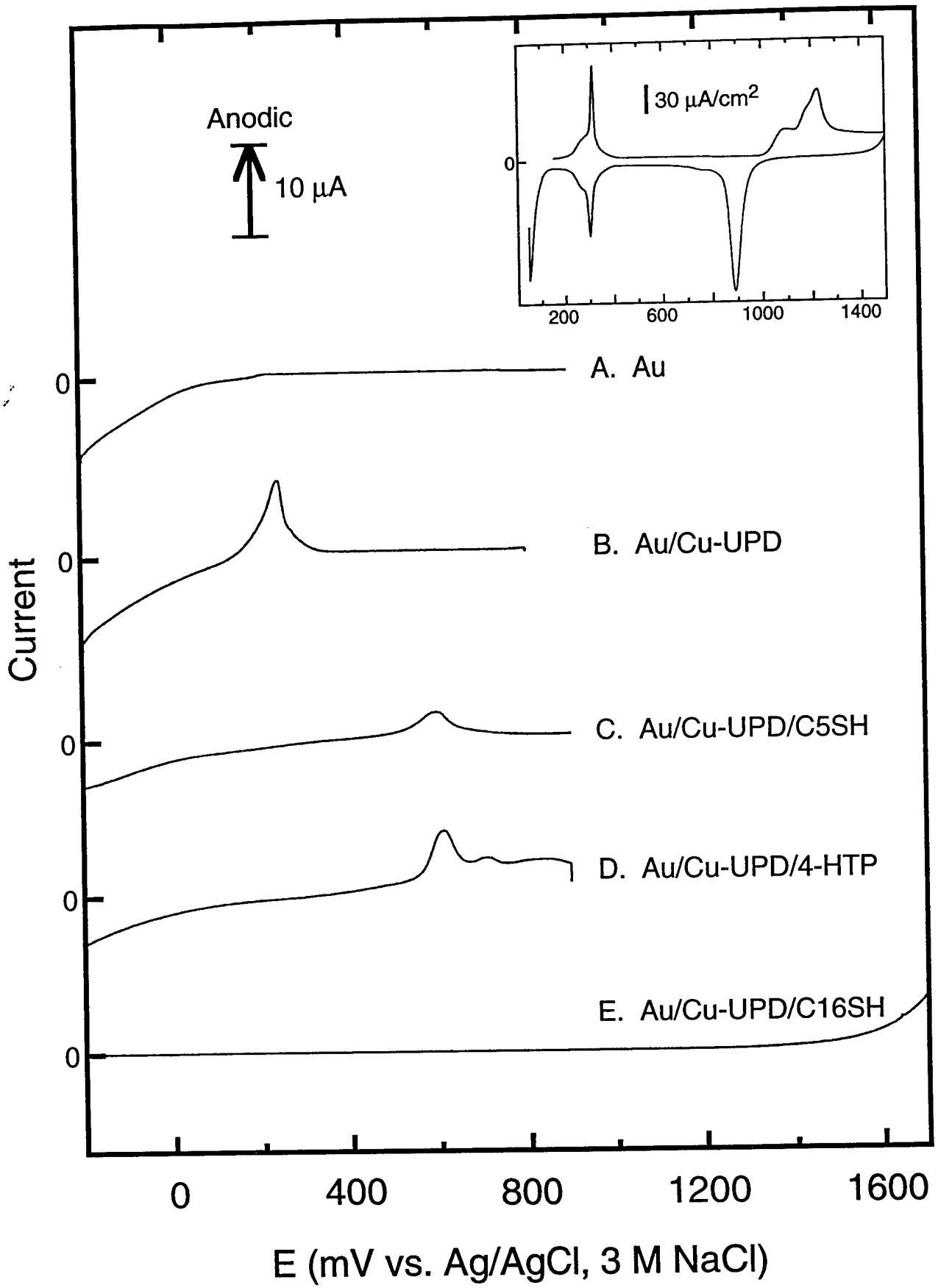

Figure 1/Zamborini, Campbell, and Crooks

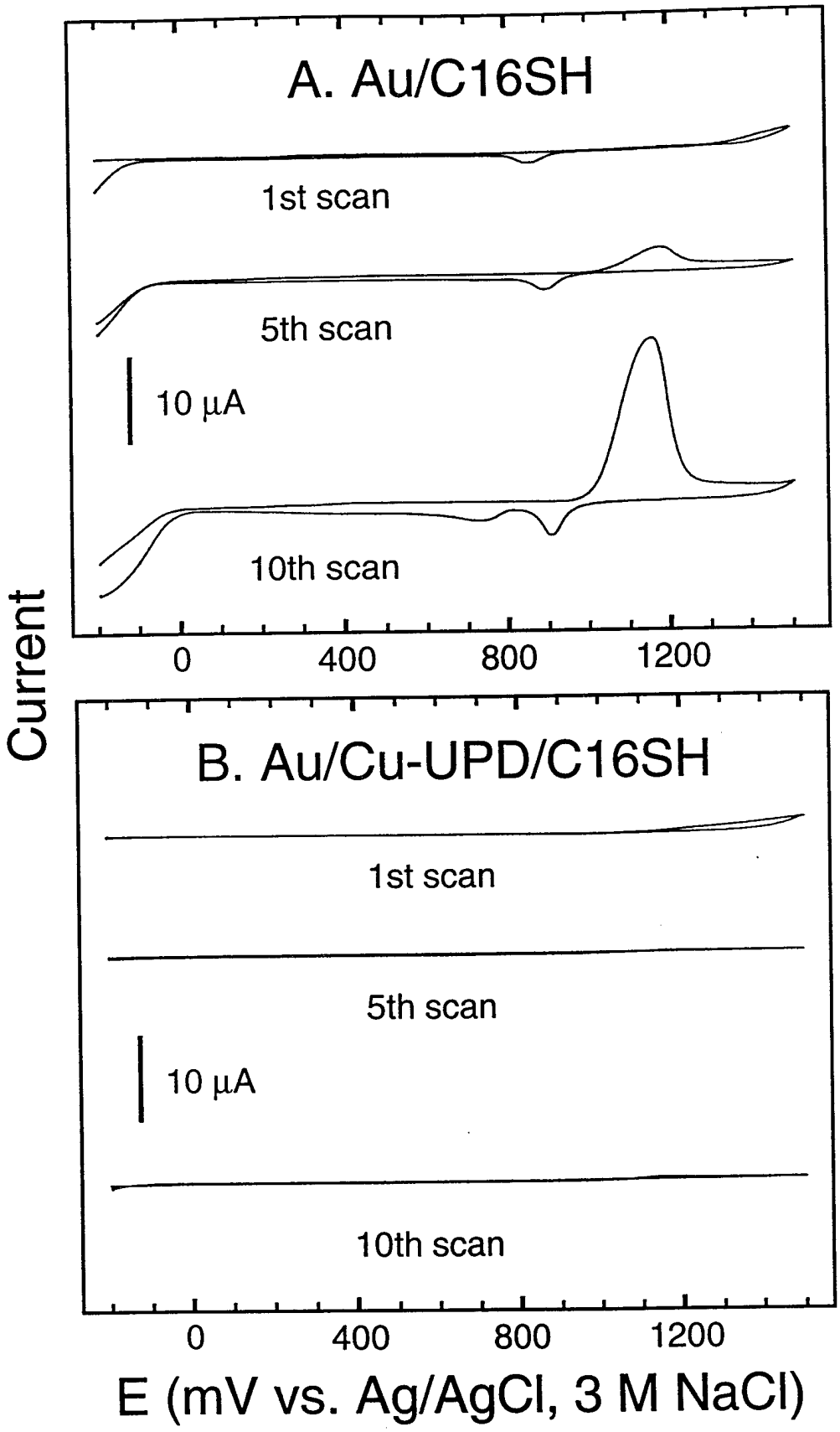

Figure 2/Zamborini, Campbell, and Crooks

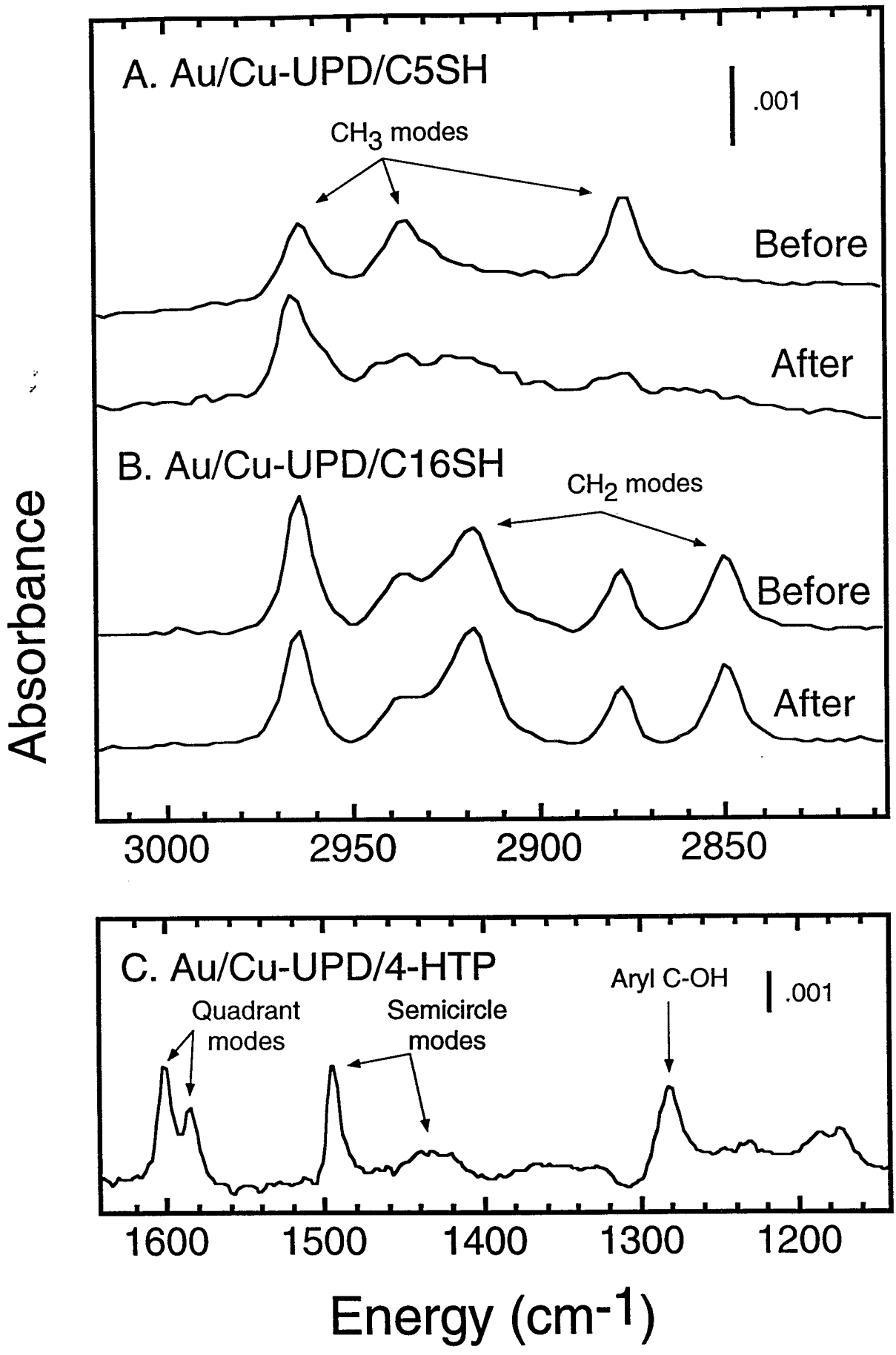

Figure 3/ Zamborini, Campbell, and Crooks

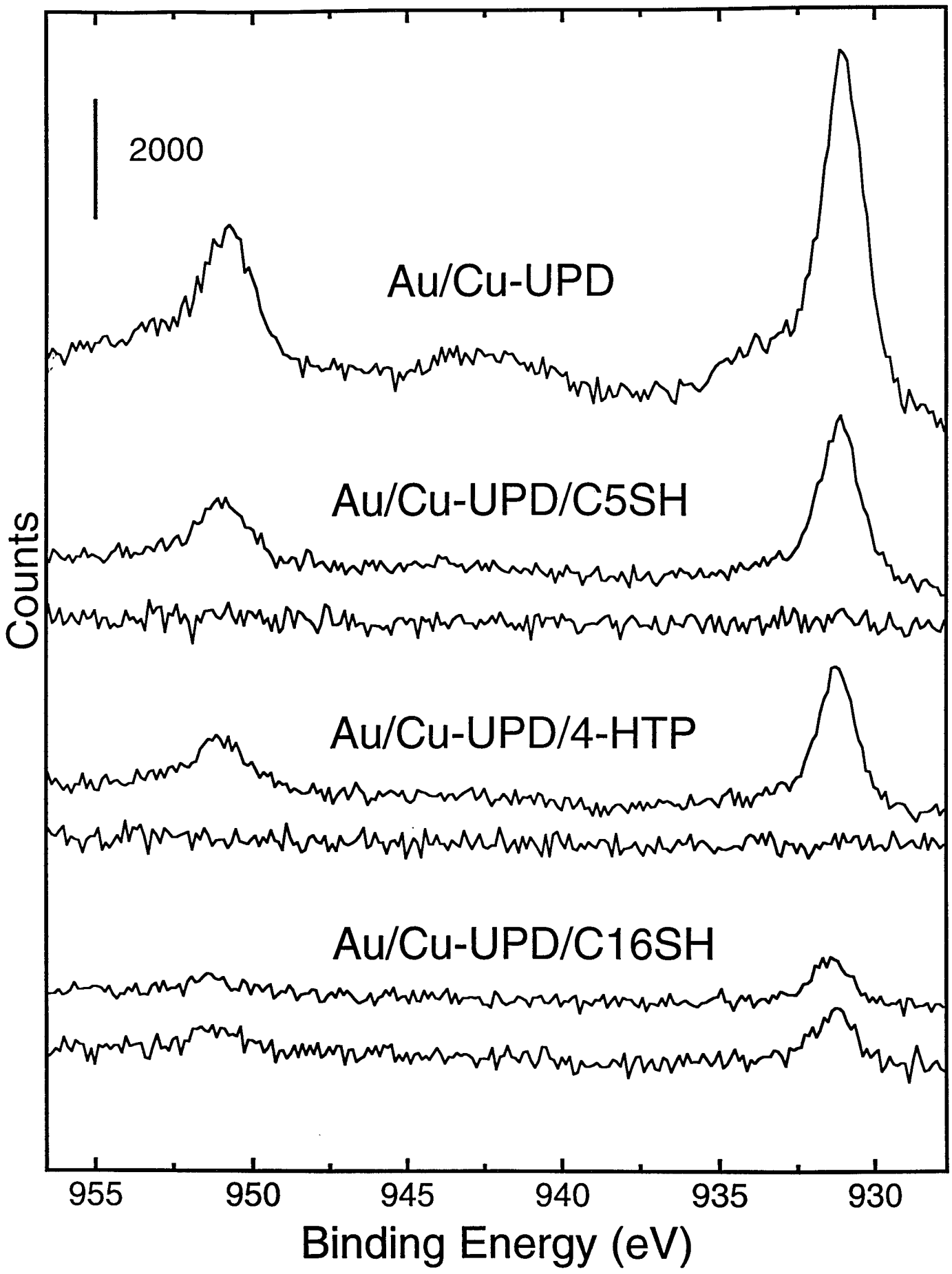

Figure 4/Zamborini, Campbell, and Crooks

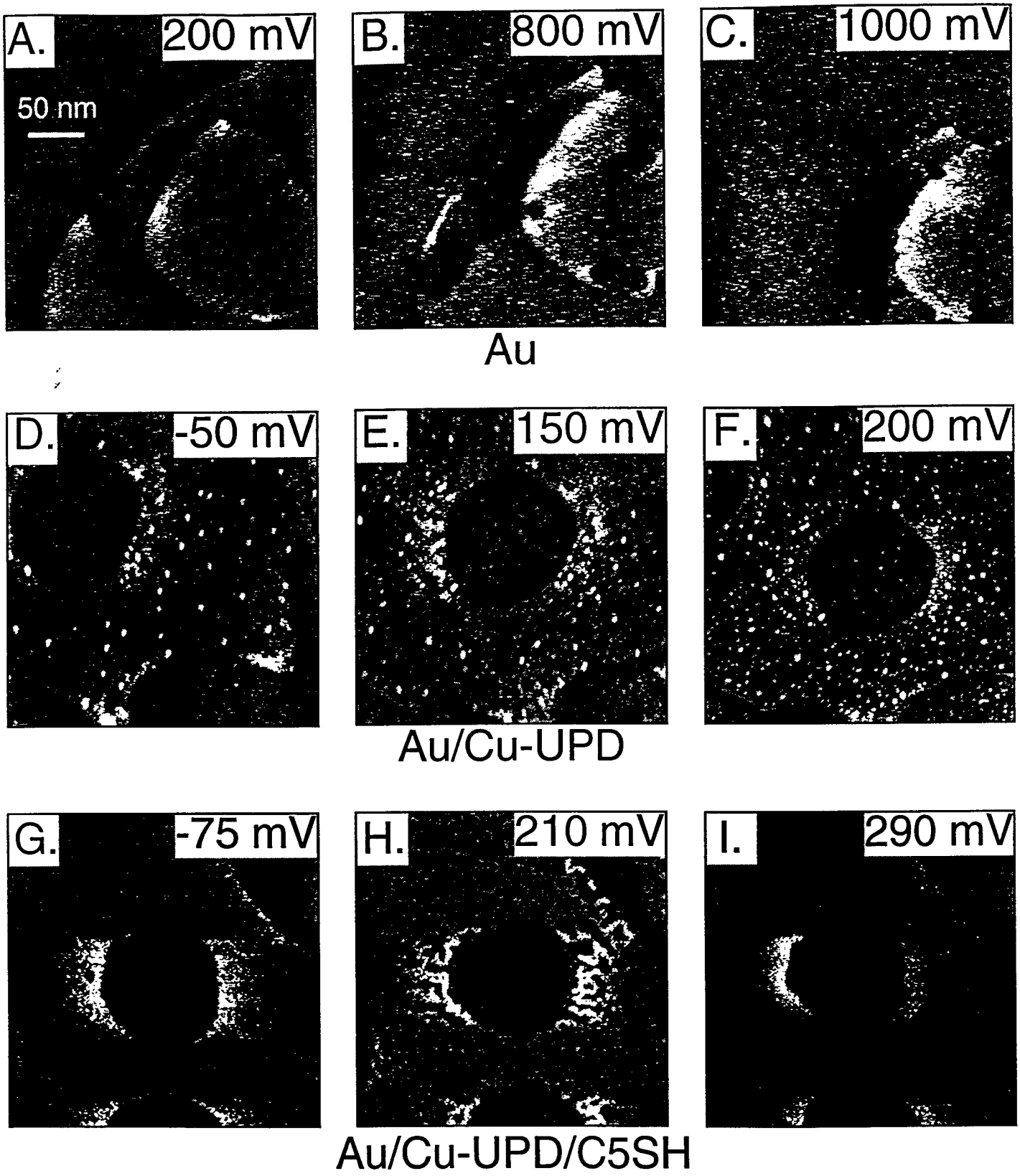

Figure 5/ Zamborini, Campbell, and Crooks

This figure continues on the next page.

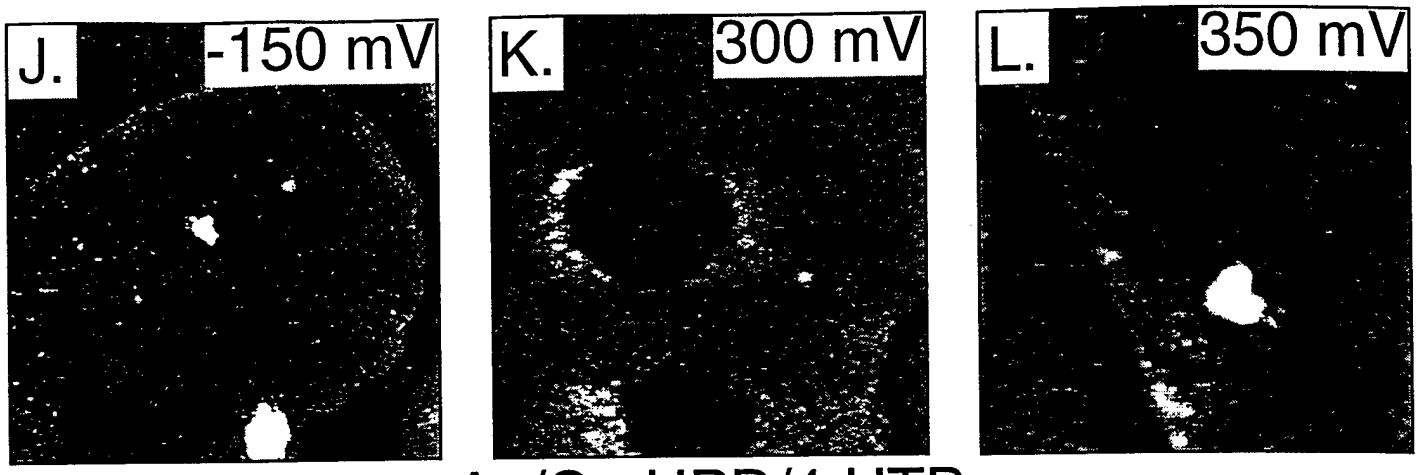

Au/Cu-UPD/4-HTP

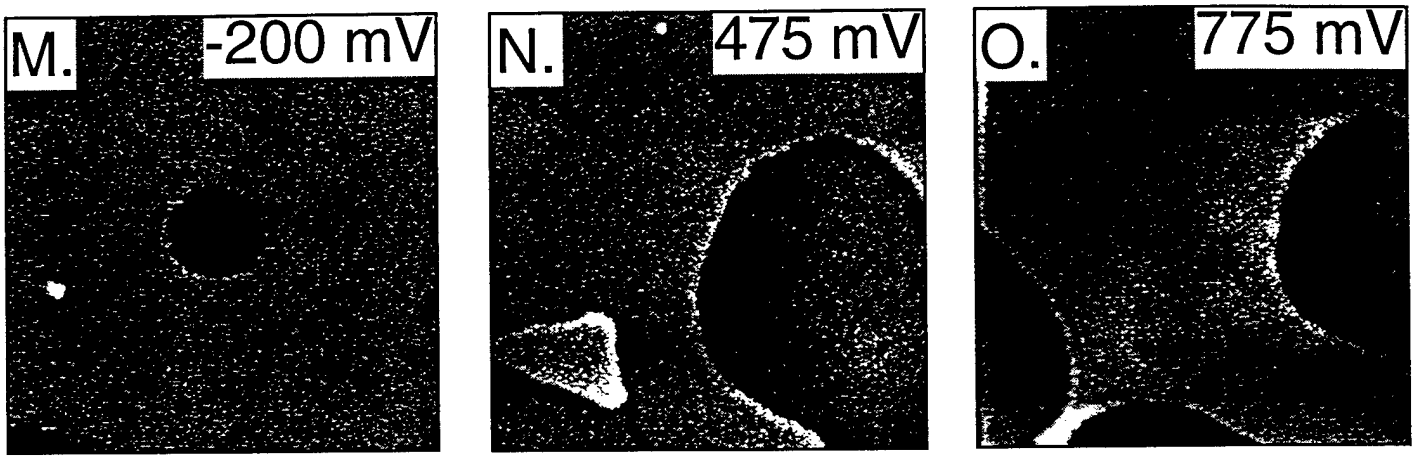

Au/Cu-UPD/C16SH

Figure 5(continued)/ Zamborini, Campbell, and Crooks

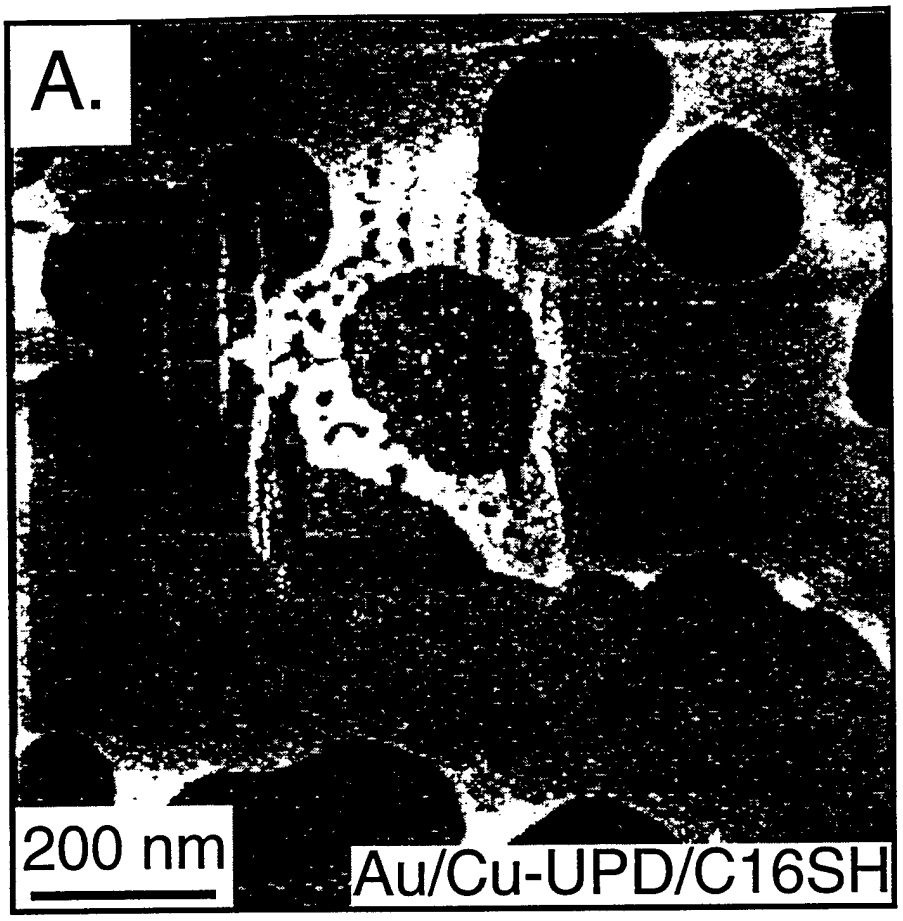

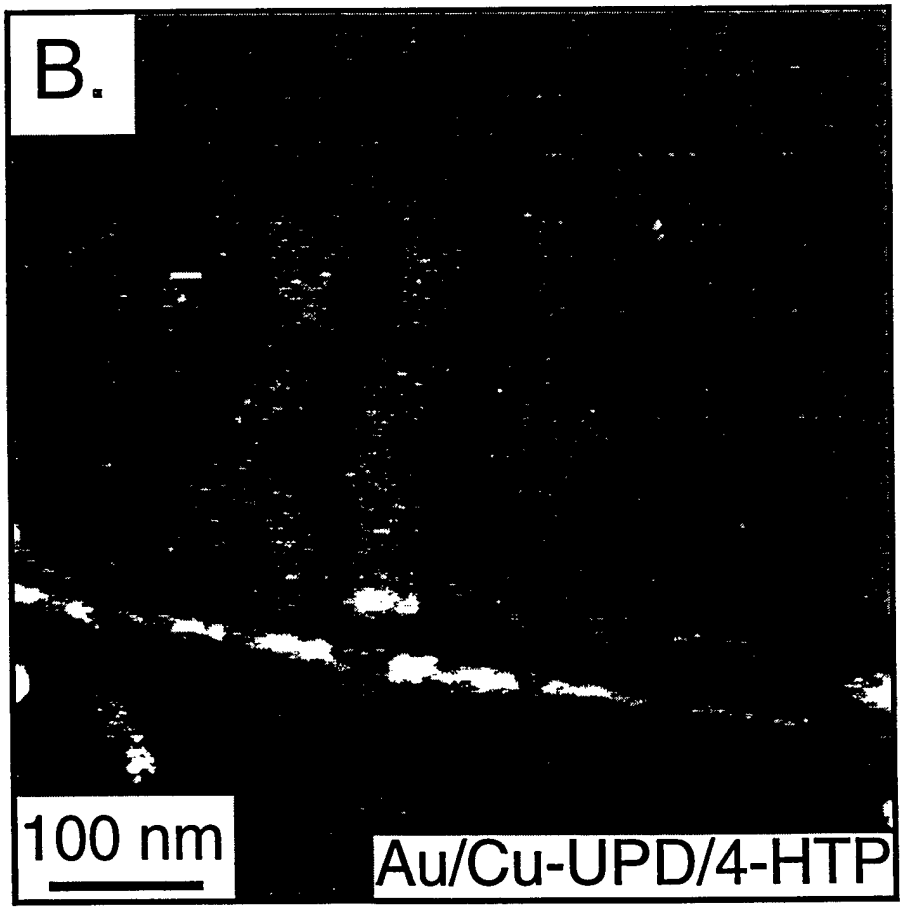

Figure 6/Zamborini, Campbell, and Crooks